Journal of Molecular Graphics and Modelling 52 (2014) 91–102

Contents lists available at ScienceDirect

Journal of Molecular Graphics and Modelling

journal homepage: www.elsevier.com/locate/JMGM

The conformational behavior, geometry and energy parameters of Menshutkin-like reaction of *O*-isopropylidene-protected glycofuranoid mesylates in view of DFT calculations

Andrzej Nowacki *, Justyna Wielińska, Dominik Walczak, Karol Sikora, Barbara Dmochowska, Beata Liberek

Faculty of Chemistry, University of Gdańsk, Wita Stwosza 63, PL-80-308 Gdańsk, Poland

ARTICLE INFO

Article history:
Accepted 23 June 2014
Available online 1 July 2014

Keywords:
Furanoid ring
Conformation
DFT calculations
NBO
Quaternary ammonium salts

ABSTRACT

The formation of pyridinium salts in the transformation of three *O*-isopropylidene-protected mesylates of furanoid sugar derivatives under pyridine action is considered at the B3LYP/6-31+G** computation level. All the structures were optimized in the gas phase, in chloroform and water. Activation barrier heights in the gas phase were also estimated at the B3LYP/6-311++G**, MPW1K/6-31+G** and MPW1K/6-311++G** levels. The conducted calculations, both in the gas phase (regardless of the computation level) and in solvents, revealed the barrier height increasing order as follows: **1** > **2** > **3** for the three reactions studied. The conformational behavior of the five-membered ring is discussed in the gas phase and in solvents. The fused dioxolane ring makes the furanoid ring less likely to undergo conformational changes. In the case of reaction **3**, the furanoid ring shape does not change either in the gas phase or in solvents. All conformers are close to E_0 or ${}^0E$.

1. Introduction

The quaternization reaction, first described by Menshutkin [1] more than one century ago, is the straightforward way of synthesizing of quaternary ammonium salts (QAS). The conceptual simplicity of this reaction, which is sometimes spurious, opens up the possibility for synthesis a wide variety of QAS from different classes of organic compounds, including derivatives of carbohydrates [2]. Although in the classic variant of the Menshutkin reaction (MR) halogen derivatives are used, the halide leaving group can be successfully replaced by a sulfonate ester [3–5].

Over the decades of experimental studies of the MR, scientists answered a number of questions regarding both the mechanics and the conditional aspects of this reaction. In particular, the nucleophile strength, the leaving group and the solvent polarity have been recognized as playing key roles. While the first two factors are important in all S_N2 reactions, the influence of the solvent polarity is of the greatest significance for the Menshutkin reaction because charged products are formed from neutral reactants.

Computational chemistry methods have delivered an alternative means of investigating the MR, which gives a deeper understanding of the problem under discussion. Many attempts have been undertaken to make a precise description of the MR with the use of theoretical chemistry methods [6–21].

Our aim is to extend the existing knowledge about the Menshutkin reaction in regard of structural features affecting its outcome. Previously, we carried out a series of studies focused on the formation of ammonium and pyridinium salts, starting from sulfonate esters of doubly substituted THF derivatives [22–26]. With the present work we continue our theoretical studies of the formation of QAS considering the reaction between pyridine and three mesylate ester derivatives (Fig. 1). The *O*-isopropylidene group is attached to the furanoid ring, which makes the THF ring with reduced freedom of motion; therefore, some of the conformations described by a pseudorotational circle seem to be inaccessible for the five-membered ring. We discuss the influence of branching both at the carbon atom next to the reaction center (the β carbon atom) and at the carbon atom three bonds distant from the reaction center (the methyl or methoxy group bounded to the furanoid ring is *cis*-oriented in relation to the reaction center carbon atom).

2. Methods

All the calculated structures were prepared in the MOLDEN program [27]. The ground state and the transition state

* Corresponding author. Tel.: +48 585235073.
E-mail address: andrzej.nowacki@ug.edu.pl (A. Nowacki).

http://dx.doi.org/10.1016/j.jmgm.2014.06.009
1093-3263/

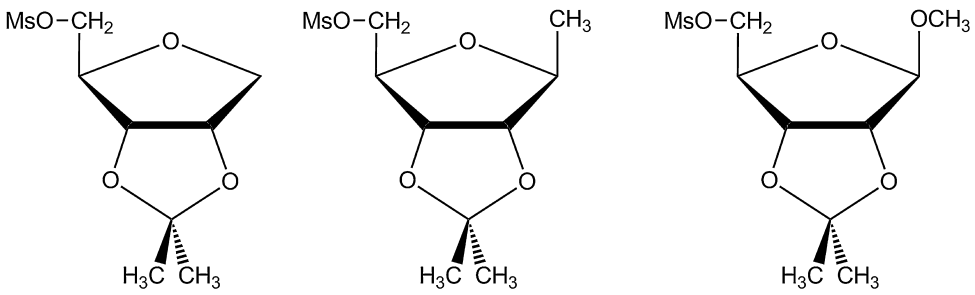

Fig. 1. Structures of mesylate derivatives converted into respective pyridinium salts.

geometries were fully optimized using density functional theory (DFT) based on Becke's three-parameter hybrid exchange [28] functional involving the gradient-corrected correlation functional of Lee, Yang and Parr [29] (B3LYP) with a 6-31+G** basis set [30,31]. The reactant complex and transition state geometries were also calculated at the B3LYP/6-311++G** level [32,33]. Reactant complexes and transition states were additionally optimized using the MPW1K (Pedrew–Wang 1-parameter model for kinetics) functional [34–36] and two basis sets: 6-31+G**, 6-311++G**.

The optimization was considered satisfactory if the energy difference between optimization cycles was less than 1×10^{-6} Hartree and a gradient of $<1 \times 10^{-4}$ a.u. was achieved. The convergence of all the systems studied was checked by harmonic vibrational analysis. No imaginary frequencies were observed for the ground state, and there was only one for the transition state. The vibrational analysis also enabled molecular entropies and thermal energy contributions for each conformer to be determined, according to statistical thermodynamics formulae.

Solvent effects were included in the calculations employing the self-consistent reaction field SCRF-PCM solvation model.[37] The reactions were studied in chloroform ($\epsilon = 4.9$) and water ($\epsilon = 78.39$) at the B3LYP/6-31+G** level. This continuum model, although not directly, accounts for the specific solvent/solute interactions (like hydrogen bonds) in some way, because the main component of such interactions has an electrostatic nature. In the PCM method the solute is placed inside a cavity generated by a series of interlocking atomic spheres. Implicit solvent calculations imply the generation of a vacuum cavity inside a continuous and homogeneous dielectric field. We used UA0 with scale factor alpha = 1.2 for water and 1.4 for chloroform [17]. The NBO analysis was carried out at the B3LYP/6-311++G** level. All calculations were done with the aid of the Gaussian 03 program [38].

3. Results and discussion

The studied reactions together with atom numbering order used in this paper are shown in Scheme 1. The steps of the reactions under consideration are as follows: two separated reactants approach one another (denoted as **R**, electrophile – mesylated derivative, and nucleophile – pyridine) which leads to the creation of the van der Waals reactant complex (**RC**) followed by its conversion into an intimate ion pair (**IP**), passing through the S_N2 saddle point structure (**TS**). Finally, the ion pair constituents are moved to an infinitely great distance (**P**) from one another.

3.1. Gas phase calculations

3.1.1. Starting geometries of the exocyclic groups

Based on our previous experience we chose the *−sc* orientation of the mesyloxy group, with respect to C3 carbon atom, as a starting geometry for the subsequent calculations (Fig. 2a). In reaction **3** we set the OCH_3 group in the *−sc* orientation, with respect to the O4 oxygen atom, in starting geometries (Fig. 2b). This geometry is preferred because of the *exo*-anomeric effect stabilization and negligible steric strains.

3.1.2. Starting geometries of the fused furanoid and dioxolane rings

Attention is continuously focused on the conformational behavior of the furanoid ring due to natural occurrence of this structural motif in biopolymers, such as DNA and RNA, and oligosaccharides

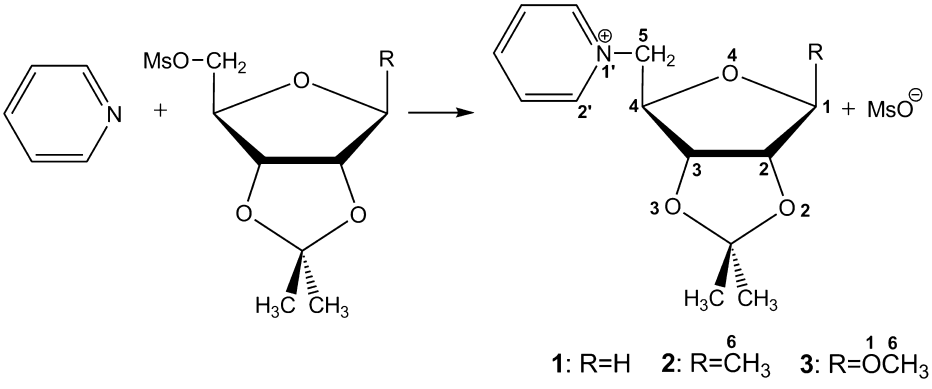

Scheme 1. Reactions of pyridinium mesylates formation.

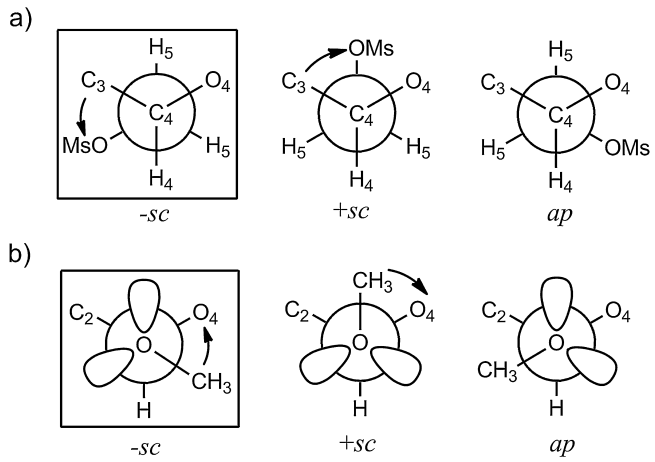

Fig. 2. Rotamers of the C4—C5 bond (a) and the O1—C1 bond (b) exhibiting possible spatial arrangements of exocyclic groups attached to the furanoid ring. The preferred orientations are these shown in boxes.

and polysaccharides, which are important components of a number of microorganisms, fungi and plants [39–42]. Knowledge about conformational preferences of the furanoid ring is vital for the evaluation of the biological activity and chemical reactivity of compounds consisting of furanoid building elements.

We assume that in molecules with *O*-isopropylidene group the furanoid ring is so much less flexible, in comparison with the unsubstituted THF ring that cannot complete a pseudorotational cycle. Such a restriction of conformational freedom of the furanoid ring was postulated for β-D-furanurono-6,3-lactones, also having a fused bicyclic structure [43].

In order to study the conformational space of the *O*-isopropylidene-protected glycofuranoid derivatives discussed in this paper it is convenient to consider the envelope shape for both rings. Since the two rings are fused, the furanoid ring has the rotational freedom related with the endocyclic oxygen atom, which can be set above or below the ring plane formed by the remaining four atoms. Similarly, the dioxolane ring conformational freedom applies to the isopropylidene carbon atom. So it seems to be reasonable to construct such geometries in which the endocyclic O atom and the isopropylidene carbon atom are moved away from the plane formed by the remaining four atoms in the furanoid and dioxolane rings, respectively. Thus, we prepared a set of initial geometries, i.e. *endo-endo*, *endo-exo*, *exo-endo* and *exo-exo* (Fig. 3), for the separate mesylate derivative (**R**), the reactant complex (**RC**), the transition state (**TS**), the ion pair (**IP**) and the separate cation (**P**). The first part of the descriptor refers to the furanoid ring, whereas the second one refers to the dioxolane ring.

3.1.3. Geometry optimization

All prepared structures were subjected to B3LYP/6-31+G** geometry optimization. The results are presented in Table 1. In the case of reactions **1** and **2**, all of the initial geometries of the separate reactants (**R**) appeared to be relatively stable. The *endo-exo* geometry is slightly preferred for **1**, although the energy differences are very small and, with one exception, are within 1 kcal mol^{-1}. (This exception refers to *exo-endo* geometry which has energy 2.24 kcal mol^{-1} higher than the *endo-exo* one.) This indicates that the individual reactant in reaction **1** may exist as a mixture mostly of three conformers, unless energy barriers are high enough to stop the conformational conversion. In turn, in reaction **2** the separate mesylate derivative with *exo-exo* geometry is the lowest in terms of energy by at least 1 kcal mol^{-1}. On the other hand, all four geometries are within 2 kcal mol^{-1}; therefore, all of them may exist in equilibrium if the energy barriers separating them are not too high. For reaction **3**, only two geometries with the furanoid ring in the *endo* form appeared to be stable, while both of *exo* conformers converted into the *endo* form upon optimization.

Again, all of the initial geometries of the reactant complex (**RC**) corresponding to reactions **1** and **2** appeared to be stable. And once again, the *endo-exo* and *exo-exo* geometries are preferred for **1** and **2**, respectively. In the case of reaction **3**, the *endo-exo* and *endo-endo* geometries of the reactant complex are relatively stable, similarly as in the separate reactants, while the two remaining starting geometries (*exo-endo* and *exo-exo*) converted into the same structures during the optimization.

In the case of transition states (**TS**) two, one and two starting geometries appeared to be stable for reactions **1**, **2** and **3**, respectively. In all of them the preferred form of the furanoid ring was the *endo* one, in which groups attached to the C1 and C4 carbon atoms approach each other. All the starting geometries of the TS having

Table 1
Relative energies (kcal mol^{-1}) of stable conformations of all characteristic points appearing along the reaction pathway optimized at the B3LYP/6-31+G** level of theory in the gas phase.

	Steps of the reaction				
	R	**RC**	**TS**	**IP**	**P**
Reaction **1**	*endo-exo*	*endo-exo*	*endo-exo*	*endo-exo*	*exo-exo*
	0.00	0.00	0.00	0.00	0.00
	endo-endo	*endo-endo*	*endo-endo*	*exo-exo*	*endo-exo*
	0.48	0.47	0.79	0.12	1.33
	exo-exo	*exo-exo*			
	0.93	1.12			
	exo-endo	*exo-endo*			
	2.24	2.36			
Reaction **2**	*exo-exo*	*exo-exo*	*endo-exo*	*exo-exo*	*exo-exo*
	0.00	0.00			
	endo-exo	*endo-exo*			
	1.12	1.01			
	exo-endo	*exo-endo*			
	1.26	1.28			
	endo-endo	*endo-endo*			
	1.73	1.49			
Reaction **3**	*endo-exo*	*endo-exo*	*endo-exo*	*endo-exo*	*endo-exo*
	0.00	0.00	0.00	0.00	0.00
	endo-endo	*endo-endo*	*endo-endo*	*exo-exo*	*exo-endo*
	0.75	0.69	0.85	1.91	4.99

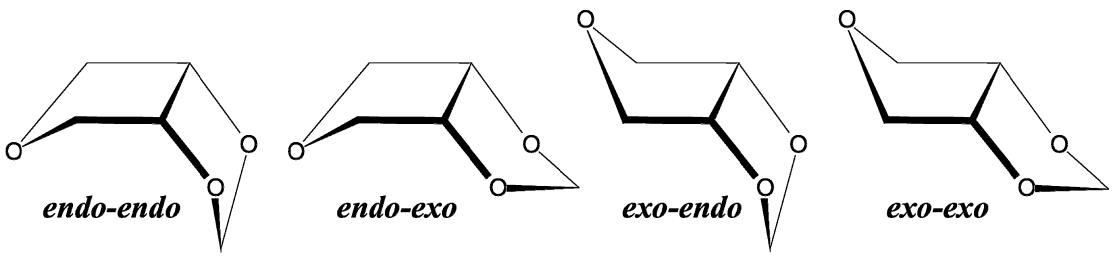

Fig. 3. Schematic presentation of *endo*/*exo* concept.

the *exo* form of the furanoid ring converted into the *endo* one during the optimization.

Also, in the case of intimate ion pairs (**IP**) and individual cations (**P**), two, one and two starting geometries appeared to be stable for reactions **1**, **2** and **3**, respectively. One can see that both geometries of the ion pair found for reaction **1** probably exist in dynamical equilibrium since the energy difference between them is only 0.12 kcal mol^{-1}. However, in the case of the individual cation of reaction **1** the *exo-exo* geometry is more stable than the *endo-exo* geometry as the energy difference is 1.33 kcal mol^{-1}. A larger energy difference between two stable forms can be observed for reaction **3**. Here the less stable conformer of the ion pair (*exo-exo*) has energy higher by 1.91 kcal mol^{-1}. In the case of the free cation the energy difference is even greater; the *exo-endo* geometry has the energy 4.99 kcal mol^{-1} higher than the *endo-exo* geometry does. Interestingly, the *exo-endo* geometry has the OCH_3 group in the *–sc* orientation, whereas in the preferred *endo-exo* geometry this group is in the unfavorable *ap* orientation (Fig. 2b). This problem will be discussed later.

An individual cation of reaction **2** has solely the *exo-exo* form. The remaining three starting structures converted into the *exo-exo* form during the optimization.

Interestingly, in all the most stable geometries, the dioxolane ring preferred the *exo* shape, in which the isopropylidene carbon atom and its substituents are more distant from the furanoid ring atoms.

3.1.4. Detailed description of the five-member ring conformation for the most stable structures occurring along the reaction pathway

The *exo*/*endo* system used above is fairly satisfactory for a rough description of the five-member ring conformations but it is unsuitable when details are needed. The conformations of five-member rings can be describe by use of the *E* (envelope) and *T* (twist) descriptors equipped with suitable indexes (superscript or/and subscript) informing which atom/s is/are moved out of the plane formed by the remaining atoms. Alternatively the description of such a ring shape can be done by defining two parameters introduced by Altona and Sundaralingam (AS), i.e. the pseudorotational phase angle (*P*) and the puckering amplitude (ϕ_m) [44,45]. The first parameter locates the exact position on the pseudorotational circle relative to the chosen conformation, whereas the second one is a measure of displacement atom(s) out of the plane.

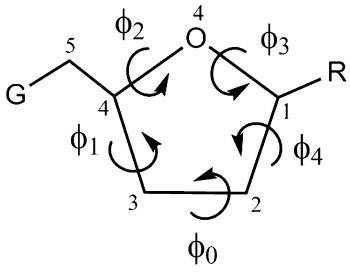

G = OMs, Py
R = H, CH_3, OCH_3

Fig. 4. Definition of the endocyclic torsion angles ϕ_0–ϕ_4.

The pseudorotational phase angle can be calculated through the use of Eq. (1), while the puckering amplitude ϕ_m from Eq. (2) [45].

$$\tan P = \frac{(\phi_2 + \phi_4) - (\phi_1 + \phi_3)}{3.077\phi_0} \quad (1)$$

$$\phi_m = \frac{\phi_0}{\cos P} \quad (2)$$

We use both these systems to describe the conformational changes of the furanoid ring that occur along the reaction pathway, because the first system (*E*/*T*), although illustrative, is less precise, especially when the furanoid ring is between the envelope and twist forms. On the other hand, it is difficult to imagine the shape of the furanoid ring basing on AS parameters only; therefore, these two conventions are complementary.

The furanoid ring conformation designations (*E* and *T*), as well as AS parameters (*P* and ϕ_m) values found for the most stable ring shapes are given in Table 2 together with the set of the endocyclic torsion angles ϕ_0–ϕ_4. The definition of these angles is shown in Fig. 4. Table 2 also lists two torsion angles (χ) describing the spatial disposition of the exocyclic groups attached to the furanoid ring. Since, in the compounds studied in this paper, both rings are fused, they are not conformationally independent, and therefore any conformational change in one of them is permanently accompanied by a suitable variation in the second. As our studies are focused on the furanoid ring, we do not consider the conformational behavior of the dioxolane ring.

Considering the most stable geometries, in reaction **1** the furanoid ring adopts the conformation lying between E_0/$^1T_0$ both in the

Table 2
Torsion angles [deg], the pseudorotational phase angle (*P*) and the puckering amplitude (ϕ_m) of the furanoid ring for the most stable geometries occurring along the reaction pathways.

			P	ϕ_m	ϕ_0	ϕ_1	ϕ_2	ϕ_3	ϕ_4	χ_1	χ_2
						Reaction **1**					
R	*endo-exo*	E_0/$^1T_0$	276	33	3.5	16.0	−31.1	33.5	−21.8	−104.1	–
RC	*endo-exo*	E_0/$^1T_0$	276	34	3.4	16.4	−31.8	34.3	−22.2	−103.6	–
TS	*endo-exo*	E_0	271	37	1.0	20.5	−35.9	36.6	−22.0	−103.2	–
IP	*endo-exo*	E_0	270	36	0.0	20.1	−34.5	34.9	−20.4	−101.7	–
P	*exo-exo*	E_4	59	37	19.0	−34.3	37.4	−24.5	1.8	−153.2	–
						Reaction **2**					
R	*exo-exo*	$^0T_1$/E_1	111	37	−13.4	−8.6	29.7	−38.3	30.9	−125.7	150.6
RC	*exo-exo*	$^0T_1$/E_1	109	38	−12.8	−9.6	30.8	−39.0	30.9	−127.1	150.8
TS	*endo-exo*	E_0/$^4T_0$	263	28	−3.2	18.7	−28.6	26.2	−13.0	−106.5	110.1
IP	*exo-exo*	E_4/$^0T_4$	67	43	−17.1	−36.7	44.1	−33.0	8.1	−154.9	127.8
P	*exo-exo*	E_4/$^0T_4$	66	39	15.6	−33.6	40.1	−29.3	6.7	−152.5	126.4
						Reaction **3**					
R	*endo-exo*	E_0	271	32	1.0	16.9	−30.4	31.1	−18.7	−103.8	102.0
RC	*endo-exo*	E_0	272	32	1.3	16.6	−30.4	31.4	−19.1	−104.1	101.9
TS	*endo-exo*	E_0/$^4T_0$	263	31	−3.9	20.7	−31.5	29.0	−14.3	−103.9	106.8
IP	*endo-exo*	E_0/$^4T_0$	261	31	−4.9	21.3	−31.7	28.8	−13.6	−101.1	107.4
P	*endo-exo*	E_0/$^1T_0$	277	31	4.3	13.7	−28.8	31.6	−21.1	−107.5	95.7

Definition of the torsion angles: χ_1, C5–C4–C3–C2 and χ_2, R–C1–C2–C3, where R represents the substituent attached to the C1 carbon atom.

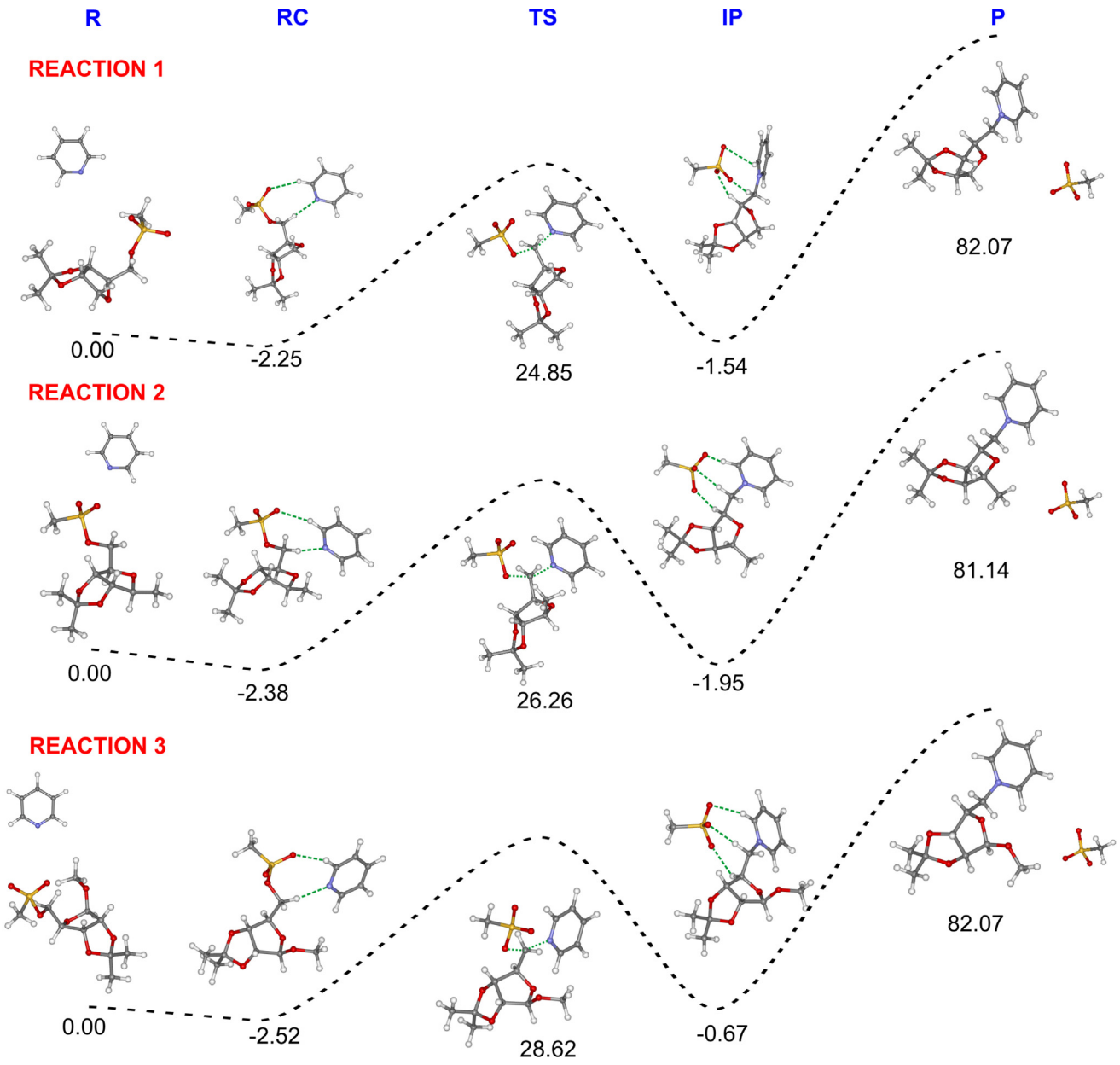

Fig. 5. Geometries of the critical points and relative energies (kcal mol^{-1}) computed at the B3LYP/6-31+G** level for reactions **1**–**3** in the gas phase.

separate mesylate derivative and in the reactant complex ($P = 276°$, $\phi_m = 33°$ and $P = 276°$, $\phi_m = 34°$, respectively, for **R** and **RC**, Table 2). Although this conformation of the furanoid ring is the most stable, it is not free of factors destabilizing it: in particular, torsion interactions resulting from nearly ecliptically oriented substituents attached to the C2 and C3 carbon atoms. Undoubtedly such a conformation owes its stability to a fused geometry as it was not preferred in the case of conformationally unrestricted derivatives with the THF ring. The fact that the E_0 conformation is preferred over the ^0E one seems to be quite surprising since the CH_2OMs group is in pseudo-axial position ($\chi_1 = -104.1°$). Consequently, this group is much closer to the hydrogen atom bounded to C1 in the E_0 conformation than in the ^0E one, which can be the source of the steric strains between this group and the hydrogen atom at C1 in the former conformation. It may be suggested that these strains are rather insignificant in this case, at least at the B3LYP level. On the other hand, the energy difference between E_0 (*endo-exo*) and ^0E (*exo-exo*) conformations is only about 1 kcal mol^{-1} (Table 1), so both of these conformers possibly exist in an equilibrium.

The preference of the furanoid ring to adopt the E_0 conformation seems to be corroborated by the transition state and the ion pair geometries. Indeed, the furanoid ring adopts the ideal E_0 conformation in the transition state ($P = 271°$, $\phi_m = 37°$). In the case of the ion pair (**IP**), the furanoid ring still takes the E_0 conformation (*endo-exo*, $P = 270°$, $\phi_m = 36°$); however, the E_4 conformation (*exo-exo*) is only 0.12 kcal mol^{-1} higher in energy, as revealed in Table 1, so the equilibrium mixture may consist of these two forms. On the other hand, in the case of the free cation (**P**), the furanoid ring takes the E_4 conformation preferentially ($P = 59°$, $\phi_m = 37°$) in which the C5 carbon atom is in a pseudo-equatorial position ($\chi_1 = -153.2°$).

A more elaborate situation is seen in reaction **2** as different conformations are observed at different stages of the reaction. Possibly, this is due to the fact that two substituents are attached to the C1 and C4 carbon atoms of the furanoid ring on the same side of this ring. Since these two groups have comparable effective size they

evoke similar conformational energy therefore more than one conformation is observed along the reaction pathway. Nevertheless, although conformations of the most stable geometries existing in the course of the reaction pathway are different, it is characteristic that all of them are gathered around ideal ^0E and E_0 shapes of the furanoid ring. This seems to confirm the increased rigidity of the furanoid ring due to the *O*-isopropylidene protecting group.

The $^0T_1/E_1$ conformation of the furanoid ring is observed in the separate reactant ($P = 111^\circ$, $\phi_m = 37^\circ$) and the reactant complex ($P = 109^\circ$, $\phi_m = 38^\circ$). In such conformation two bulky groups (CH_2OMs and CH_3) are in pseudo-equatorial orientation ($\chi_1 \sim -126^\circ$, $\chi_2 \sim 151^\circ$, Table 2), so they are moved away from one another avoiding the steric hindrance.

The opposite – with respect to the separate reactant and the reactant complex – conformation of the furanoid ring is observed in the transition state of reaction **2**. Here the furanoid ring adopts the intermediate $E_0/^4T_0$ conformation ($P = 263^\circ$, $\phi_m = 28^\circ$), in which the CH_2OMs and CH_3 groups are in pseudo-axial positions ($\chi_1 = -106.5^\circ$, $\chi_2 = 110.1^\circ$, Table 2). It should be stressed here that it is the only stable geometry for this transition state.

Another conformational change is observed on going downhill from the transition state to the intimate ion pair product. The intermediate $E_4/^0T_4$ conformation ($P = 67^\circ$, $\phi_m = 43^\circ$) is preferred by the furanoid ring for this structure. Actually, this conformation is similar to that found for the reactant complex and the separate reactant. Also in this conformation the CH_2OMs and CH_3 groups are in pseudo-equatorial orientation ($\chi_1 = -154.9^\circ$, $\chi_2 = 127.8^\circ$, Table 2) as a result they are moved away one another. The same conformation is adopted by the furanoid ring in free cation.

In the case of reaction **3** the furanoid ring stays practically unchanged in the whole process. In the separate reactant the furanoid ring adopts the E_0 conformation ($P = 271^\circ$, $\phi_m = 32^\circ$). The same conformation is observed in the reactant complex. A certain conformational change is seen on going from the reactant complex to the transition state geometry. Here the furanoid ring takes the intermediate $E_0/^4T_0$ conformation ($P = 263^\circ$, $\phi_m = 31^\circ$) and keeps it in the ion pair. Another insignificant change happens when the constituents of the ion pair are separated to an infinite distance, giving individual ions. This process is accompanied by the $E_0/^4T_0 \rightarrow E_0/^1T_0$ conformational transformation of the furanoid ring.

3.1.5. Energy parameters and geometry changes near the reaction center

The gas phase results of the B3LYP/6-31+G** calculations for reactions **1**, **2** and **3** are presented in Table 3. Optimized geometries together with relative energies corresponding to all the stationary points along the reaction pathway are presented in Fig. 5. The relative energies refer to the sum of the separate reactant energies. The energies were corrected with zero-point vibrational energy (ZPVE). A scaling factor of 0.9877 was used to correct for the well-known systematic error in the vibrational zero point energy [46].

According to the B3LYP/6-31+G** computational level (Table 3 and Fig. 5), the complexation process occurs with a small reduction in energy ($\Delta E = -2.5$ kcal mol^{-1} on average). Such an energy value is quite characteristic for the formation of these types of complexes. Comparable values of the complexation energy were observed for reactions discussed in our earlier papers, in particular for the reaction between pyridine and mesylate derivatives that did not bear the 3,4-*O*-isopropylidene group restricting the conformational flexibility of the furanoid ring [23,24]. In turn, the Gibbs free energy predicts the complexation process to be unfavorable (~7.0 kcal mol^{-1} on average) in all cases.

The low value of the complexation energy indicates that the constituents of the reactant complex are held together due to rather weak interactions, mainly O···H—C and N···H—C hydrogen bonding contacts [47], shown in Fig. 6. The existence of such

Table 3
Geometry parameters, relative energies and relative Gibbs free energies of the relevant stationary points on the PES in the gas phase calculated at the B3LYP/6-31+G** level for reactions **1**–**3**.

	Reaction 1					Reaction 2					Reaction 3				
	(R)	**(RC)**	**(TS)**	**(IP)**	**(P)**	**(R)**	**(RC)**	**(TS)**	**(IP)**	**(P)**	**(R)**	**(RC)**	**(TS)**	**(IP)**	**(P)**
d(C—O)	1.439	1.464	2.057	3.099	∞	1.453	1.464	2.057	3.252	∞	1.457	1.466	2.063	3.100	∞
d(C—N)	∞	3.467	2.088	1.496	1.493	∞	3.503	2.096	1.496	1.493	∞	3.517	2.093	1.497	1.486
Δ*d*	−∞	−2.003	−0.031	1.603	∞	−∞	−2.039	−0.039	1.756	∞	−∞	−2.051	−0.030	1.603	∞
∠OCN	–	104.2	162.0	94.0	–	–	100.6	161.0	88.3	–	–	104.2	158.5	92.3	–
A	−68.6	−68.5	25.3	−168.3	−178.4	−70.1	−69.2	22.0	172.7	−178.7	−72.9	−72.8	9.5	−167.2	172.7
B	–	–	178.9	–	–	–	–	−179.9	–	–	–	–	179.7	–	–
C	–	–	–	–	–	–	–	–	–	–	−67.9	−66.4	−68.2	−72.4	−157.6
D	–	157.8	154.1	133.5	102.0	–	164.4	156.6	108.6	101.4	–	164.2	161.0	138.2	95.3
Δ*E*	0.00	−2.25	24.85	−1.54	82.07	0.00	−2.38	26.26	−1.95	81.14	0.00	−2.52	28.62	−0.67	82.07
Δ*G*	0.00	6.70	37.03	10.72	83.23	0.00	7.64	39.56	11.65	83.30	0.00	6.70	40.69	11.49	83.95

All energy values in kcal mol^{-1}, *d* in Å and angles in deg. Reaction coordinate: Δ*d* = *d*(C—O) – *d*(C—N). (**R**) – separate reactants, (**RC**) – reactant complex, (**TS**) – transition state, (**IP**) – ion pair and (**P**) – separate ions.
A, torsion angle: (O–C5–C4–C3) for **R**, **RC** and **TS**; (N–C5–C4–C3) for **IP** and **P**.
B, deformation angle C4–C5–H5–H5′ describing the planarity of the transition state geometry. See Fig. 7.
C, torsion angle defining the position of the methyl group in relation to the furanoid ring (H_3C–O1–C1–O4).
D, torsion angle describing the orientation of the pyridine ring in relation to the C5—C4 bond (C2′–N–C5–C4).

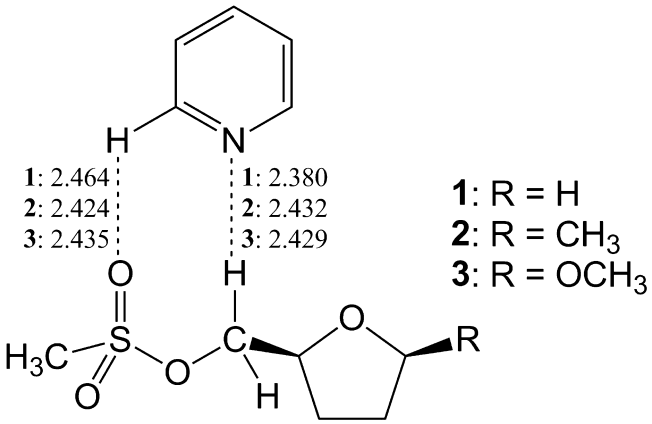

Fig. 6. Hydrogen bonding interactions stabilizing the reactant complexes. Distances between the hydrogen atom and the acceptor are given in Å.

interactions between the constituents of the reactant complex was corroborated basing on the NBO analysis (Table S1). The suitable second-order perturbation energies $E^{(2)}$ (donor → acceptor) that involve $\sigma^*_{(C-H)}$ antibonds indicate that the N and O lone pairs participate as donors whereas the $\sigma^*_{(C-H)}$ antibonds as acceptors in intermolecular charge transfer interactions, $n_X \rightarrow \sigma^*_{(C-H)}$.

An inspection of data collected in Table 3 shows that the geometries of the transition states of all the reactions are quite similar. The C···O and C···N distances are almost identical in all three transition states. Also, the values of the O···C···N valence angle are roughly the same. In the case of reactions **1** and **2** this angle value is about 162°, whereas it is approximately 4° less in reaction **3**. The values of this angle clearly indicate that the nucleophilic nitrogen atom, the reaction center carbon atom and the oxygen atom being the part of leaving group are not in a straight line. This is in contrast to previously studied reactions of methyl mesylate/halide (reactants were not branched at the β position) in which three atoms: N, C and O, were ideally in a straight line [22,23,25,26].

The approach of the pyridine molecule to the C5 carbon atom induces considerable O–C5–C4–C3 torsion angle changes within the mesylate derivative in the transition state (**A**, Table 3). In reactant complexes this angle takes values characteristic for the staggered −*sc* conformation (Fig. 2a) with the O–C5–C4–C3 torsion angle value of about −70°. For the transition state geometries obtained for reactions **1** and **2** the O–C5–C4–C3 torsion angle adopts values closer to the +*sc* conformation (25.3° and 22.0° for **1** and **2**, respectively) whereas it is 9.5° for reaction **3**. Thus, in the case of reactions **1** and **2** the mesylate leaving group is positioned over the furanoid ring. In turn, in reaction **3**, breaking the C5—O bond is almost in an ecliptic position with respect to the C4—C3 bond which could explain the slightly greater deviation of the O···C···N valence angle in this case.

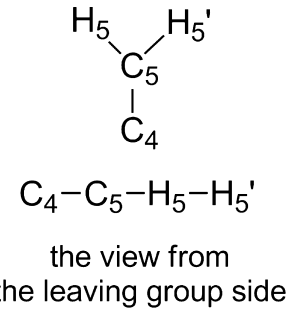

Fig. 7. Definition of the deformation angle.

We use the deformation angle, defined in Fig. 7, to judge the dilemma of the early/late character of the transition state. This angle shows whether the atoms (or the entire substituents) attached to the reaction center carbon are located in one plane in the transition state geometry. It is commonly accepted that this angle should be close to 180° for the ideal S_N2 transition state. Any deviation from this value indicates the pyramidal disposition of the substituents bonded with the reaction center carbon atom in the transition state geometry. Additionally, the sign of this angle indicates whether Walden inversion of the ligands bonded to the reaction center carbon atom has occurred or not. According to the proposed convention the negative value means that the ligands are before Walden inversion (the early transition state), whereas the positive value means that the inversion has been done (the late transition state).

The values of the deformation angle presented in Table 3 (the angle **B**) are very close to 180° which indicate that all ligands attached to the reaction center carbon atom are in the same plane, hence the transition state geometry is exactly halfway between the reactant complex and the ion pair for all reactions studied in vacuum. The same conclusion was drawn in the case of analogous reactions in which the mesylate derivative had the THF ring with unrestricted conformational flexibility [23,24].

The gas phase relative energy values matching the transition states with respect to the separated reactants are given in Table 3, and the activation barriers relating to the reactant complexes are listed in Table 4. Comparing the results in Table 4, one can see that the lowest barrier is for reaction **1** whereas the highest barrier is for reaction **3**. The differentiation of barrier heights corroborates our statement about the importance of branching at the C1 carbon atom. The lowest barrier is found when the hydrogen atom is attached to the C1 carbon atom (reaction **1**). The presence of the hydrogen atom bonded to the C1 carbon atom in *cis* orientation with respect to the reaction center carbon atom, permits the rotation about C5—C4 bond and locates the leaving group in conformation close to +*sc* (Fig. 2a). This rotation makes the TS geometry less crowded thus helps to reduce the barrier height. A slightly higher barrier is found for reaction **2** in which the CH_3 group is attached to the C1 carbon atom. In this case, the TS geometry also has the leaving group in the conformation close to +*sc*. This may indicate that the repulsion between the OMs leaving group and the CH_3 group is not very strong. The highest barrier is found for reaction **3**, where the OCH_3 group is attached to the C1 carbon atom. In this case the breaking MsO—C5 bond is nearly in ecliptic conformation with respect to the C3—C4 bond. It seems that apart for steric strains (not very strong in fact), the electrostatic repulsion between the partially released OMs group and glycosidic oxygen atom (O1) blocks the rotation about the C5—C4 bond, disabling the staggered conformation adoption and hence increasing the barrier of reaction **3** with respect to reaction **2**.

We have found the same order of barrier heights regardless the calculation level, although barriers obtained from the MPW1K level of calculations are higher by about 3 kcal mol^{-1} than those from the B3LYP calculations. Data in Table 3 clearly show that barriers calculated with aid of the greater basis set are roughly the same; therefore, we conclude that the extension of the basis set is pointless in our case.

Some surprising findings arise from the comparison of the activation barriers presented here with those published earlier [23,24]. First of all the introduction of the *O*-isopropylidene protecting group to the molecule of the reactant leads to a certain reduction of the barrier height, particularly in the case of reaction **1**. Moreover, the barrier found for reaction **1** is even lower, by about 1 kcal mol^{-1}, than the respective barrier calculated for the reaction of methyl mesylate with pyridine.[23] This means that the effect – constantly observed in our studies – of the barrier height increase induced by

Table 4
Activation energies calculated for reactions **1**–**3** in the gas phase. All energy values in kcal mol^{-1}.

	B3LYP				MPW1K			
	6-31+G**		6-311++G**		6-31+G**		6-311++G**	
	$\Delta E^{\ddagger}$	$\Delta G^{\ddagger}$	$\Delta E^{\ddagger}$	$\Delta G^{\ddagger}$	$\Delta E^{\ddagger}$	$\Delta G^{\ddagger}$	$\Delta E^{\ddagger}$	$\Delta G^{\ddagger}$
Reaction **1**	27.42	30.33	27.02	29.95	30.09	33.51	29.85	32.83
Reaction **2**	28.64	31.92	28.05	30.97	31.45	35.46	31.11	34.35
Reaction **3**	31.15	33.99	30.61	33.12	34.33	37.17	34.05	36.77

the branching at the C4 atom (a β position with respect to the reaction center carbon atom) does not work here. Also, the restriction of the conformational flexibility of the furanoid ring is not the source of the higher barrier, as might be expected.

Ion pairs formed during the reaction are less stable than the respective reactant complexes in the gas phase, although the energy value differences are rather insignificant (1.03 kcal mol^{-1}, 0.43 kcal mol^{-1} and 1.85 kcal mol^{-1} for reactions **1**, **2** and **3**, respectively, Table 3). These results are in contrast to our previous studies, in which the ion pairs had lower energy than the respective reactant complexes [23,24].

In the final stage of the reaction, the ions formed during the reaction course move to an infinite distance from one another. As always, the separation of the constituents of the ion pair is strongly endergonic in the gas phase. In all the reactions studied the energy that must be supplied to complete this process exceeds 80 kcal mol^{-1}, with respect to separate reactants.

A separate discussion is necessary for the individual cation geometry (**P**) formed in reaction **3**. The two geometries (*endo-exo* and *exo-endo*) of B3LYP optimized free cations for reaction **3** are presented in Fig. 8a and b. These two geometries significantly differ in energy (about 5 kcal mol^{-1}) but also in the conformation of both five-membered rings and the spatial orientation of the OCH_3 group. Interestingly, the geometry with the OCH_3 group located in accordance with the *exo*-anomeric effect (*exo-endo*) has the higher energy than the *endo-exo* geometry which is not stabilized by the *exo*-anomeric effect. Therefore, the question arises as to why the *exo-endo* geometry, which is stabilized by the *exo*-anomeric effect, is much less favorable than the *endo-exo* one. We think that two factors make the *endo-exo* geometry preferred: (1) the intramolecular C(Py)—H···O1 hydrogen bonding interaction and (2) the *endo*-anomeric effect. As can be seen in Fig. 8, such a hydrogen bonding interaction is possible for *endo-exo* geometry and the *ap* orientation of the CH_3 group (Fig. 2b). Indeed, in the *endo-exo* geometry the distance between the pyridine ring hydrogen atom and the glycosidic O1 atom is only 2.308 Å (Fig. 8a) whereas it increased to 4.022 Å while the rings shapes were reverse (*exo-endo* geometry, Fig. 8b). In turn, the *endo*-anomeric effect stabilization results here from the pseudo-axial orientation of aglycone with respect to the furanoid ring being in the $E_0/{}^1T_0$ conformation (Table 2). To corroborate our statements we calculated one more geometry for the free cation having the *endo-exo* rings shapes (Fig. 8c). In this new geometry the OCH_3 group is oriented in accordance with the *exo*-anomeric effect requirement, whereas the pyridine moiety is turned to another staggered orientation thus avoiding the C(Py)—H···O1 hydrogen bonding interaction. This geometry appeared to be 4.04 kcal mol^{-1} higher in energy than the global minimum, proving the crucial role of the C(Py)—H···O1 hydrogen bonding interaction in stabilizing of the individual cation geometry.

The other evidence for the C(Py)—H···O1 hydrogen bonding interactions stabilizing the free cation comes from the NBO analysis (Table S2). It can be seen that $\sigma^*_{(C-H)}$ antibonds occupation number in the *endo-exo* geometry is much higher, in comparison with *exo-endo* one. It should be also noted that the O lone pairs occupation number differ from the ideal occupation by an important amount. These results can be rationalized in terms of intramolecular interactions of charge transfer from the oxygen lone pairs to the $\sigma^*_{(C-H)}$ antibonds. The second-order perturbation energies $E^{(2)}$ indicate that the O lone pairs participate as donors and the $\sigma^*_{(C-H)}$ antibonds as acceptors in intramolecular charge transfer interactions, $n_O \rightarrow \sigma^*_{(C-H)}$. Lack of the respective $E^{(2)}$ value indicate that the intramolecular C(Py)—H···O1 hydrogen bonding interaction is not formed in *exo-endo* geometry.

Although the preferred geometry of the ion pair found for reaction **3** has almost the same shape of two five-membered rings as the free cation (*endo-exo* geometry), the OCH_3 group is in *−sc* orientation that fulfills the *exo*-anomeric effect requirement in the ion pair. Clearly the geometries of the ion pair and the individual cation differs so profound from one another that the respective C(Py)—H···O1 hydrogen bonding interaction cannot be formed in the former.

3.2. Solvent calculations

3.2.1. Energy parameters and geometry changes

To estimate the effects of the solvents on the reactions under scrutiny a polarizable continuum model (PCM) developed by Tomasi et al. [37] was used. We carried out the optimization of all geometries found on the reaction course in two solvents, i.e. chloroform and water. The results of calculations in both solvents are listed in Table 5, and the energy diagrams comparing the energy profiles for the gas phase and two solvents are presented in Fig. 9. The energy parameters of the reactions studied in solvents are expressed by the so-called pseudochemical potential (U_0) [48] and Gibbs free energy (G).

The presented energy diagrams reveal significant differences for reactions taking place in various environments, in particular on the product side (ion pairs and separated ions). On the other hand, the energy differences on the reactant side and in the transition state point are rather minor for different environments. In chloroform the reactant complexes are less stabilized by about 1 kcal mol^{-1} than the respective ones in the gas phase. In the water medium reactant complexes appeared to be of the same stability as individual reactants. In turn, the Gibbs free energy values clearly indicate that the complexation process is strongly unfavorable for all cases, regardless of the environment in which it occurs.

The B3LYP/6-31+G** level barriers calculated in solvents are lower than those calculated for the gas phase. For reaction **1** the barrier ($\Delta U_0^{\ddagger}$) is lower by about 2.6 kcal mol^{-1} and 4.9 kcal mol^{-1}, when it takes place in chloroform and water, respectively (Tables 4 and 5). Analogous energy barrier height reduction is observed for two other reactions.

As in the gas phase, a certain differentiation of the energy barriers can be observed also in solvents depending on the kind of substituent bonded to the C1 carbon atom, being in *cis* orientation with respect to the reaction center carbon atom (C5). Both, in chloroform and water medium, the lowest barrier is found for reaction **1**, in which the mesylate molecule has the hydrogen atom bonded to the C1 carbon atom. In the case of reaction **3** (with the OCH_3 group at the C1 atom) the barrier is the highest in both solvents. This observation corroborates our earlier finding that two factors, i.e.

Table 5
Geometry parameters, relative energies and relative Gibbs free energies of relevant stationary points on the FES at the B3LYP/6-31+G** level, calculated for reactions **1**–**3** in chloroform and water.

	Reaction **1**					Reaction **2**					Reaction **3**				
	(**R**)	(**RC**)	(**TS**)	(**IP**)	(**P**)	(**R**)	(**RC**)	(**TS**)	(**IP**)	(**P**)	(**R**)	(**RC**)	(**TS**)	(**IP**)	(**P**)
								Chloroform							
d(C—O)	1.455	1.465	2.026	3.201	∞	1.454	1.465	2.029	3.309	∞	1.457	1.467	2.034	3.178	∞
d(C—N)	∞	3.475	2.122	1.491	1.490	∞	3.505	2.127	1.493	1.490	∞	3.512	2.126	1.494	1.485
Δd	−∞	−2.010	−0.096	1.710	∞	−∞	−2.040	−0.098	1.816	∞	−∞	−2.045	−0.092	1.684	∞
∠OCN	–	104.3	164.2	94.8	–	–	101.3	163.1	89.7	–	–	104.8	160.9	93.6	–
A	−69.1	−68.0	31.2	−174.2	−179.4	−69.8	−69.0	26.0	169.9	−179.4	−72.1	−72.6	14.3	−167.4	177.5
B	–	–	−178.6	–	–	–	–	−177.5	–	–	–	–	−177.5	–	–
C	–	–	–	–	–	–	–	–	–	–	−68.5	−66.7	−68.6	−75.2	−89.1
D	–	156.6	143.7	117.4	102.0	–	161.8	149.3	100.6	99.0	–	163.4	154.7	125.6	85.2
ΔU_0	0.00	−1.38	23.44	−6.13	18.48	0.00	−1.31	24.93	−5.78	17.65	0.00	−1.53	27.15	−4.89	20.20
ΔG	0.00	7.66	35.07	5.84	19.41	0.00	7.65	37.14	6.48	19.14	0.00	7.56	38.78	7.65	21.03
$\Delta U_0^{\ddagger}$			24.82					26.25					28.68		
$\Delta G^{\ddagger}$			27.41					29.49					31.22		
								Water							
d(C—O)	1.457	1.466	1.996	3.297	∞	1.456	1.465	1.999	3.415	∞	1.459	1.468	2.000	3.271	∞
d(C—N)	∞	3.506	2.159	1.487	1.488	∞	3.568	2.161	1.489	1.488	∞	3.529	2.176	1.492	1.485
Δd	−∞	−2.040	−0.163	1.810	∞	−∞	−2.112	−0.162	1.926	∞	−∞	−2.070	−0.176	1.779	∞
∠OCN	–	104.2	165.0	95.4	–	–	102.1	164.6	88.4	–	–	104.6	162.1	93.9	–
A	−69.5	−67.7	35.7	−179.2	178.1	−70.4	−68.7	31.3	170.1	178.6	−72.4	−72.6	18.0	−169.4	−178.3
B	–	–	−175.4	–	–	–	–	−174.9	–	–	–	–	−173.2	–	–
C	–	–	–	–	–	–	–	–	–	–	−68.5	−67.3	−68.0	−77.1	−80.3
D		155.0	131.0	105.8	94.4		162.1	132.9	94.7	94.3		162.2	150.6	122.0	77.6
ΔU_0	0.00	−0.12	22.34	−12.45	−6.60	0.00	−0.03	23.77	−12.52	−7.84	0.00	−0.29	25.48	−10.48	−5.25
ΔG	0.00	8.86	34.96	−0.29	−5.55	0.00	8.72	36.86	0.12	−7.02	0.00	8.00	36.72	0.95	−4.60
$\Delta U_0^{\ddagger}$			22.46					23.80					25.78		
$\Delta G^{\ddagger}$			26.09					28.15					28.72		

All energy values in kcal mol^{-1}, d in Å and angles in deg. Reaction coordinate: $\Delta d = d$(C—O) − d(C—N). (**R**), separate reactants; (**RC**), reactant complex; (**TS**), transition state; (**IP**), ion pair; (**P**), separate ions.
A, torsion angle: (O–C5–C4–C3) for **R**, **RC** and **TS**; (N–C5–C4–C3) for **IP** and **P**.
B, deformation angle C4–C5–H5–H5′ describing the planarity of the transition state geometry. See Fig. 7.
C, torsion angle defining the position of the methyl group in relation to the furanoid ring (H_3C–O1–C1–O4).
D, torsion angle describing the orientation of the pyridine ring in relation to the C5—C4 bond (C2′–N–C5–C4).

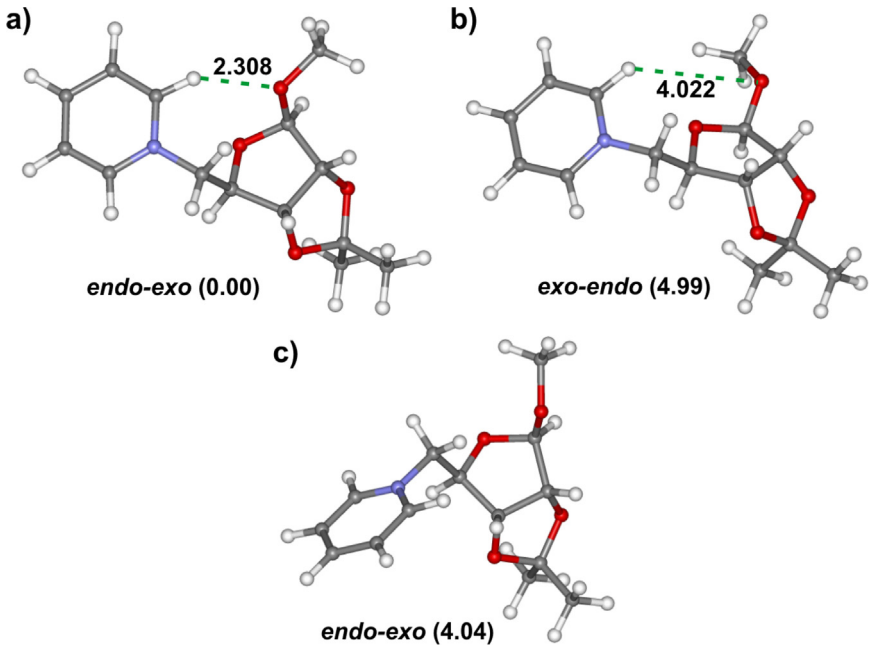

Fig. 8. Comparison of individual cation structures calculated for reaction **3** at the B3LYP/6-31+G** level. Distances between the hydrogen atom and the acceptor are given in Å.

steric and electrostatic repulsion, affect the barrier height. It seems that in the case of reaction **2**, the steric strains between the partially released leaving group and methyl group attached to the C1 carbon atom is the only factor increasing the barrier size in comparison to reaction **1**.

It can be seen that some geometry parameters changes occurred during the optimization of the transition state geometry in solvents. The C···N distance elongated and the C···O distance has shortened, while the polarity of the environment increased, although the changes were not significant. In chloroform the C···N distance increased and the C···O distance decreased by about 1.5% on average, in relation to the reference values from the gas phase. In water the changes of these distances were more or less twice as big as in chloroform, being still quite insignificant. The direction of these changes give the evidence that in both solvents the transition state geometries are shifted toward the earlier stage of the reaction with respect to the gas phase. The same conclusion can be drawn from the analysis of the deformation angle (**B**, Table 5). All the values of this angle are negative; therefore, the transition state geometries are more reactant-like in both solvents. Such a behavior of the TS geometries is characteristic for the reactions in which charge separation occurs along the reaction pathway.

The values of the torsion angle **A** found in the transition state geometries optimized in both solvents are very similar to those obtained in the gas phase. The differences are within 10° of each other.

The next point on the reaction pathway is the ion pair. This point represents a stable structure, i.e. no spontaneous dissociation of the ion pair is observed in the reactions under consideration. This is in contrast with the result presented by Castejon [6]. According to both ΔU_0 and ΔG, the bimolecular conversion of reactant complexes into ion pairs is accompanied by an energy decrease with respect to the reactant complex in solvents, which is in contrast to the gas phase results. Particularly in water, the energy reduction is considerable; the ion pair is lower in energy than the respective reactant complex by at least 10 kcal mol^{-1} (Table 5). In chloroform this effect is not so profound. In fact, the Gibbs free energy difference between the reactant complex and the ion pair is zero in the case of reaction **3**.

The final step of the reaction, i.e. separation of the constituents of the ion pair to infinite distance, requires much less energy to be completed in chloroform with regard to the gas phase; however, still this process is unfavorable, according to both pseudochemical potential (U_0) and the Gibbs free energy. A very different situation

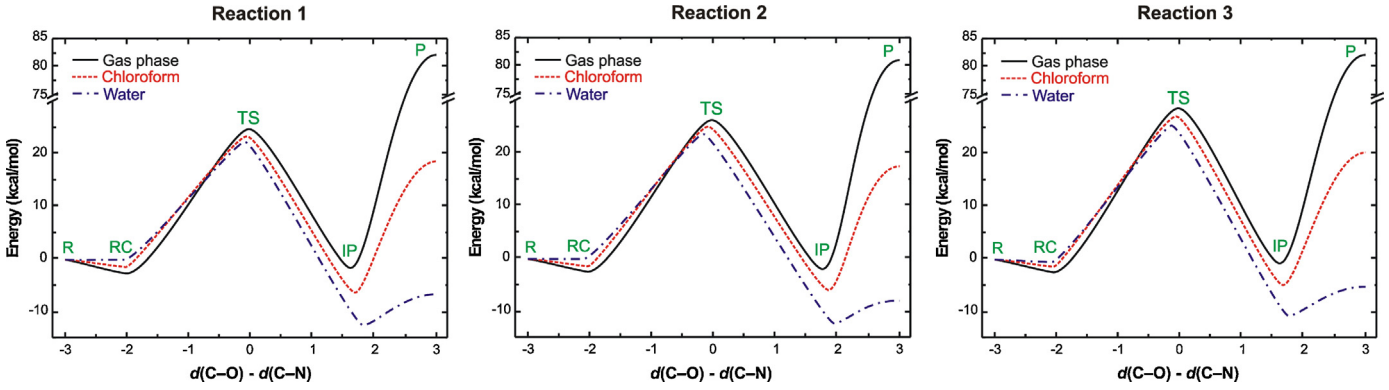

Fig. 9. Comparison of energy and pseudochemical potential (U_0) profiles for reactions **1**–**3** in the gas phase, chloroform and water.

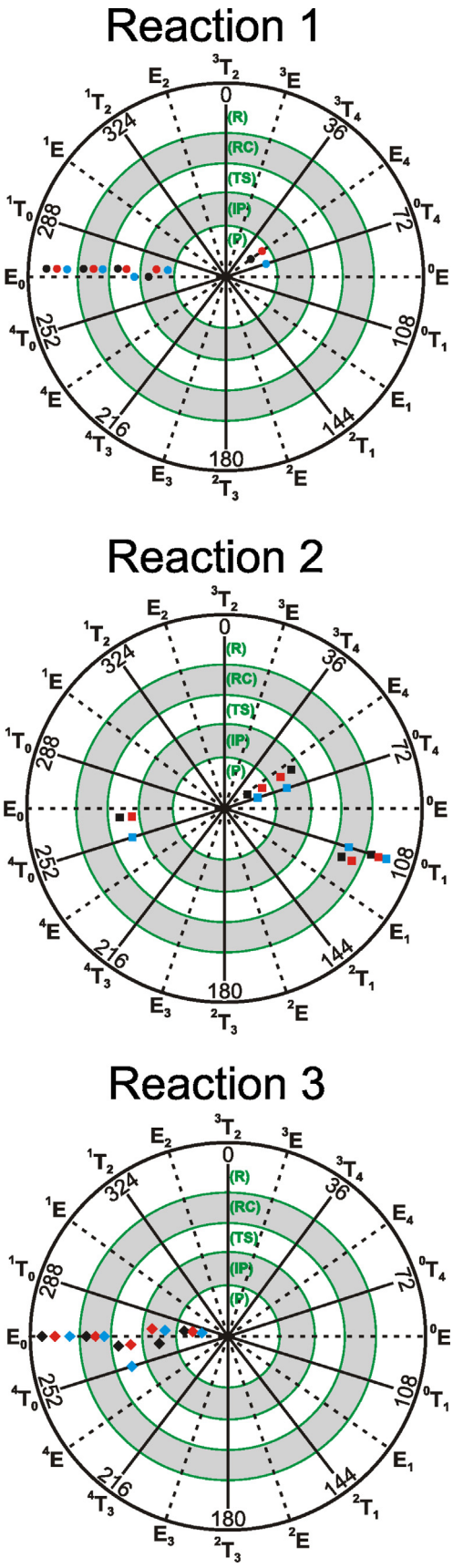

Fig. 10. Distribution of the furanoid ring conformations in a pseudorotational circle for the most stable geometries found in the reaction pathways in the gas phase (black) and in solvents: chloroform (red) and water (blue). (For interpretation of the references to color in this figure legend, the reader is referred to the web version of the article.)

is found in water medium. In this solvent the separation of the ions is accompanied by an energy increase (U_0); on the other hand, the Gibbs free energy values indicate that dissociation of the ion pair should be favorable (Table 5).

It is noteworthy that for reaction **3** the free cation has the OCH_3 group constantly located in *–sc* orientation (Fig. 2b) in both solvents. This may indicate that the C—H···O1 hydrogen bonding interaction found in the gas phase is of minor significance in solvents.

3.2.2. *Furanoid ring conformation in solvents*

The optimization in solvents does not show significant changes of the furanoid ring conformation, as can be seen in Fig. 10. Separate reactants and reactant complexes have approximately the same conformation of the furanoid ring in the gas phase and in solvents (E_0 for reactions **1** and **3**; $^0T_1$ for reaction **2**). A certain divergence can be seen for other points, particularly TSs; however, they are observed in water medium only. This finding proves the increased rigidity of the furanoid ring protected by the isopropylidene group.

4. Conclusions

DFT studies on the Menshutkin-like reaction between pyridine and three mesylate esters of *O*-isopropylidene furanoid derivatives were carried out in this work. We compared results obtained in the gas phase and in two solvents of different polarity: chloroform and water.

We carried out conformational analysis of the furanoid ring of all characteristic points occurring along the reaction pathway. We noticed that the most stable conformations are close to E_0 or ^0E for reaction **2**. In the case of reaction **1** the furanoid ring adopts predominantly conformations close to E_0. In turn, this ring adopts exclusively conformations close to E_0 for reaction **3**. This finding demonstrates that the furanoid ring has restricted conformational freedom due to the *O*-isopropylidene protecting group. In the furanoid ring protected in this way only the endocyclic oxygen atom has a certain movement possibility; therefore, the conformations found are near to E_0 or ^0E, which are located on the east and the west regions of the pseudorotational circle, respectively. Conformations from the north and south poles of the pseudorotational circle have been avoided for the currently studied compounds. Interestingly, the E_0 conformation is preferred for TSs in all reactions studied. Possibly, this conformation enables the best arrangement of five groups around the reaction center carbon atom.

We also investigated the bifurcation at the C1 carbon atom – the energy barrier height relationship. Once again we showed that the energy barrier is sensitive to the presence of the substituent bonded to the C1 carbon atom, *cis* oriented with respect to the reaction center carbon atom (C5). Thus, the following order of reactivity is observed in our studies: **1** > **2** > **3** in the gas phase and in both solvents.

Comparing the gas phase activation barriers presented here with those published previously, we have noticed that introduction of the *O*-isopropylidene protecting group to the molecule of the reactant caused a certain reduction of the barrier height, particularly in the case of reaction **1.** Moreover, the barrier found for reaction **1** is lower, by about 1 kcal mol^{-1}, than the respective barrier calculated for the reaction of methyl mesylate with pyridine.

Activation barriers were estimated using the B3LYP and MPW1K functionals with two basis sets: 6-31+G** and 6-311++G**. It has been shown that extending the basis set is pointless in our studies, as the barriers found at the two theory levels appeared to be roughly the same. The MPW1K calculations predict the barriers to be higher by about 3 kcal mol^{-1} than those from B3LYP/6-31+G**

calculations. Nevertheless, the trend of the reactivity is the same, regardless the functional used.

The early/late character of the transition state geometry correlates well with the environment polarity. Based on the broken/formed bonds and deformation angle analysis we conclude that a more product-like transition state found in the gas phase shifts toward the early (reactant-like) TS in water.

Relative energy and relative Gibbs free energy values indicate that the overall process is highly unfavorable in the gas phase. In chloroform it is still unfavorable, but in water the sum of the energies of individual ions are less (ΔU_0) than that of the separate reactants.

Acknowledgements

This research work was supported by DS/530-8451-D382-14, BMN/538-8450-B349-14 and the system project "InnoDoktorant – Scholarships for PhD students, VIth edition" (K. Sikora). Project is co-financed by the European Union in the frame of the European Social Fund. All DFT calculations were carried out using the resources of the Informatics Centre of the Metropolitan Academic Network in Gdańsk (CI TASK).

Appendix A. Supplementary data

Supplementary data associated with this article can be found, in the online version, at http://dx.doi.org/10.1016/j.jmgm.2014.06.009.

References

[1] N. Menschutkin, Z. Phys. Chem. 5 (1890) 589–601.
[2] E. Fischer, K. Raske, Chem. Ber. 43 (1910) 1750–1753.
[3] V. Kumar, C.E. Olsen, S.J.C. Schäffer, V.S. Parmar, S.V. Malhotra, Org. Lett. 9 (2007) 3905–3908.
[4] B. Dmochowska, E. Skorupa, P. Świtecka, A. Sikorski, I. Łącka, S. Milewski, A. Wiśniewski, J. Carbohydr. Chem. 28 (2009) 222–233.
[5] M.D.R. Gomes da Silva, M.M.A. Pereira, Carbohydr. Res. 346 (2011) 197–202.
[6] H. Castejon, K.B. Wiberg, J. Am. Chem. Soc. 121 (1999) 2139–2146.
[7] J.W. Viers, J.C. Schug, M.D. Stovall, J.I. Seeman, J. Comput. Chem. 5 (1984) 598–605.
[8] M. Solà, A. Lledós, M. Duran, J. Bertrán, J.-L.M. Abboud, J. Am. Chem. Soc. 113 (1991) 2873–2879.
[9] J. Gao, X. Xia, J. Am. Chem. Soc. 115 (1993) 9667–9675.
[10] U. Maran, T.A. Pakkanen, M. Karelson, J. Chem. Soc. Perkin Trans. 2 (1994) 2445–2452.
[11] S. Shaik, A. Ioffe, A.C. Reddy, A. Pross, J. Am. Chem. Soc. 116 (1994) 262–273.
[12] X. Fradera, L. Amat, A.M. Torrent, J. Mestres, P. Constans, E. Besalú, J. Martí, S. Simon, M. Lobato, J.M. Oliva, J.M. Luis, M. Andrés, M. Solà, R. Carbó, M. Duran, J. Mol. Struct. (Theochem) 371 (1996) 171–183.
[13] T.N. Truong, T.-T.T. Truong, E.V. Stefanovich, J. Chem. Phys. 107 (1997) 1881–1889.
[14] U. Maran, M. Karelson, T.A. Pakkanen, J. Mol. Struct. (Theochem) 397 (1997) 263–272.
[15] C. Amovilli, B. Mennucci, F.M. Floris, J. Phys. Chem. B 102 (1998) 3023–3028.
[16] S.P. Webb, M.S. Gordon, J. Phys. Chem. 103 (1999) 1265–1273.
[17] J. Poater, M. Solà, M. Duran, X. Fradera, J. Phys. Chem. A 105 (2001) 6249–6257.
[18] A. Melo, A.J.I. Alfaia, J.C.R. Reis, A.R.T. Calado, J. Phys. Chem. B 110 (2006) 1877–1888.
[19] A. Fábián, F. Ruff, Ö. Farkas, J. Phys. Org. Chem. 21 (2008) 988–996.
[20] R. Bini, C. Chiappe, C.S. Pomelli, B. Parisi, J. Org. Chem. 74 (2009) 8522–8530.
[21] O. Acevedo, W.L. Jorgensen, J. Phys. Chem. B 114 (2010) 8425–8430.
[22] A. Nowacki, B. Dmochowska, E. Jączkowska, K. Sikora, A. Wiśniewski, Comput. Theor. Chem. 973 (2011) 53–61.
[23] A. Nowacki, B. Dmochowska, K. Sikora, J. Madaj, A. Wiśniewski, Comput. Theor. Chem. 986 (2012) 85–92.
[24] A. Nowacki, K. Sikora, B. Dmochowska, A. Wiśniewski, Comput. Theor. Chem. 1000 (2012) 33–41.
[25] A. Nowacki, K. Sikora, B. Dmochowska, A. Wiśniewski, J. Mol. Model 19 (2013) 3015–3026.
[26] D. Walczak, A. Nowacki, J. Mol. Model 19 (2013) 4403–4417.
[27] G. Schaftenaar, J.H. Noordik, J. Comput.-Aided Mol. Des. 14 (2000) 123–134.
[28] A.D. Becke, J. Chem. Phys. 98 (1993) 5648–5652.
[29] C. Lee, W. Yang, R.G. Parr, Phys. Rev. B 37 (1988) 785–789.
[30] W.J. Hehre, R. Ditchfield, J.A. Pople, J. Chem. Phys. 56 (1972) 2257–2261.
[31] T. Clark, J. Chandrasekhar, G.W. Spitznagel, P.v.R. Schleyer, J. Comput. Chem. 4 (1983) 294–301.
[32] A.D. McLean, G.S. Chandler, J. Chem. Phys. 72 (1980) 5639–5648.
[33] R. Krishnan, J.S. Binkley, R. Seeger, J.A. Pople, J. Chem. Phys. 72 (1980) 650–654.
[34] B.J. Lynch, P.L. Fast, M. Harris, D.G. Truhlar, J. Phys. Chem. A 104 (2000) 4811–4815.
[35] B.J. Lynch, D.G. Truhlar, J. Phys. Chem. A 105 (2001) 2936–2941.
[36] Y. Zhao, J. Pu, B.J. Lynch, D.G. Thuhlar, Phys. Chem. Chem. Phys. 6 (2004) 673–676.
[37] J. Tomasi, M. Persico, Chem. Rev. 94 (1994) 2027–2094.
[38] M.J. Frisch, G.W. Trucks, H.B. Schlegel, G.E. Scuseria, M.A. Robb, J.R. Cheeseman, J.A. Montgomery Jr., T. Vreven, K.N. Kudin, J.C. Burant, J.M. Millam, S.S. Iyengar, J. Tomasi, V. Barone, B. Mennucci, M. Cossi, G. Scalmani, N. Rega, G.A. Petersson, H. Nakatsuji, M. Hada, M. Ehara, K. Toyota, R. Fukuda, J. Hasegawa, M. Ishida, T. Nakajima, Y. Honda, O. Kitao, H. Nakai, M. Klene, X. Li, J.E. Knox, H.P. Hratchian, J.B. Cross, V. Bakken, C. Adamo, J. Jaramillo, R. Gomperts, R.E. Stratmann, O. Yazyev, A.J. Austin, R. Cammi, C. Pomelli, J.W. Ochterski, P.Y. Ayala, K. Morokuma, G.A. Voth, P. Salvador, J.J. Dannenberg, V.G. Zakrzewski, S. Dapprich, A.D. Daniels, M.C. Strain, O. Farkas, D.K. Malick, A.D. Rabuck, K. Raghavachari, J.B. Foresman, J.V. Ortiz, Q. Cui, A.G. Baboul, S. Clifford, J. Cioslowski, B.B. Stefanov, G. Liu, A. Liashenko, P. Piskorz, I. Komaromi, R.L. Martin, D.J. Fox, T. Keith, M.A. Al-Laham, C.Y. Peng, A. Nanayakkara, M. Challacombe, P.M.W. Gill, B. Johnson, W. Chen, M.W. Wong, C. Gonzalez, J.A. Pople, Gaussian 03, Revision D.02, Gaussian, Inc., Wallingford, CT, 2004.
[39] T.Y. Nikolaienko, L.A. Bulavin, D.M. Hovorun, J. Biomol. Struct. Dyn. 29 (2011) 563–575.
[40] T.Y. Nikolaienko, L.A. Bulavin, D.M. Hovorun, Phys. Chem. Chem. Phys. 14 (2012) 15554–15561.
[41] J.B. Houseknecht, T.L. Lowary, J. Org. Chem. 67 (2002) 4150–4164.
[42] H.A. Taha, M.R. Richards, T.L. Lowary, Chem. Rev. 113 (2013) 1851–1876.
[43] B. Liberek, D. Tuwalska, I. do Santos-Zounon, A. Konitz, A. Sikorski, Z. Smiatacz, Carbohydr. Res. 341 (2006) 2275–2285.
[44] C. Altona, M. Sundaralingam, J. Am. Chem. Soc. 94 (1972) 8205–8212.
[45] J.B. Houseknecht, C. Altona, C.M. Hadad, T.L. Lowary, J. Org. Chem. 67 (2002) 4647–4651.
[46] M.P. Andersson, P. Uvdal, J. Phys. Chem. A 109 (2005) 2937–2941.
[47] U. Koch, P.L.A. Popelier, J. Phys. Chem. 99 (1995) 9747–9754.
[48] Y. Kim, J.R. Mohring, D.G. Truhlar, J. Am. Chem. Soc. 132 (2010) 11071–11082.